ACS APPLIED MATERIALS & INTERFACES

Research Article

www.acsami.org

Amphiphilic (Phthalocyaninato) (Porphyrinato) Europium Triple-Decker Nanoribbons with Air-Stable Ambipolar OFET Performance

Guang Lu,[†] Xia Kong,[‡] Pan Ma,[§] Kang Wang,[†] Yanli Chen,*[,‡] and Jianzhuang Jiang*[,†]

[†]Beijing Key Laboratory for Science and Application of Functional Molecular and Crystalline Materials, Department of Chemistry, University of Science and Technology Beijing, Beijing 100083, China

[‡]School of Science, China University of Petroleum (East China), Qingdao 266580, China

[§]Jinan Academy of Agricultural Sciences, Jinan 250316, China

Supporting Information

ABSTRACT: An amphiphilic mixed (phthalocyaninato) (porphyrinato) europium(III) triple-decker complex [Pc(OPh)$_8$]Eu[Pc(OPh)$_8$]Eu[TP(C≡CCOOH)PP] (**1**) with potential ambipolar semiconducting HOMO and LUMO energy levels has been designed, synthesized, and characterized. The OFET devices fabricated by quasi-Langmuir-Shäfer (QLS) technique at the air/water interface with nanoparticle morphology display hole mobility of 7.0×10^{-7} cm^2 V^{-1} s^{-1} and electron mobility of 7.5×10^{-7} cm^2 V^{-1} s^{-1}, which reflects its ambipolar semiconducting nature. However, the performance of the devices fabricated via a "phase-transfer" method from *n*-hexane with one-dimensional nanoribbon morphology was significantly improved by 3−6 orders of magnitude in terms of hole and electron mobilities, 0.11 and 4×10^{-4} cm^2 V^{-1} s^{-1}, due to the enhanced $\pi-\pi$ interaction in the direction perpendicular to the tetrapyrrole rings associated with the formation of a dimeric supramolecular structure building block depending on the intermolecular hydrogen bonding between the neighboring triple-decker molecules in the one-dimensional nanoribbons.

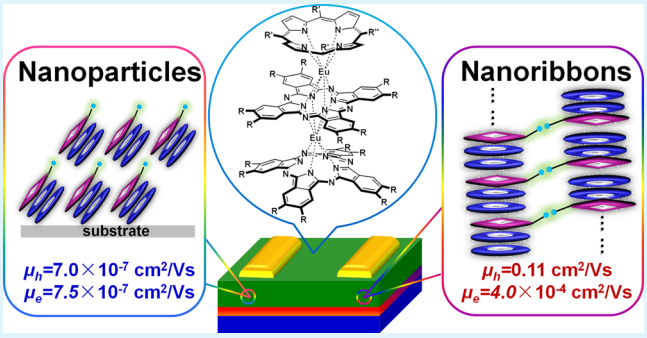

KEYWORDS: *phthalocyanine, triple-decker, ambipolar, OFET, 1-D nanoribbons*

INTRODUCTION

Development of organic field-effect transistors (OFETs) has gotten great research interest in the past decades due to its potential applications in low-cost integrated circuits and flexible electronics.[1−3] As a result, great effort has been made to develop novel organic semiconductor materials with high carrier mobility and good solubility in common organic solvents such as conjugated polymers, oligomers of thiophenes, and phthalocyanines.[4−11] During the aforementioned strive, many observations have suggested that both the packing model and maximizing π-orbital overlap between neighboring conjugated molecules in the self-assembled nanostructures of organic semiconductor are very important for the purpose of achieving high carrier mobility.[12−16] Henceforth, a wide range of effective approaches have been developed to enhance the intermolecular coupling of conjugated semiconductor molecules in self-assembled nanostructures through modifying the molecular structure and programming the supramolecular interaction, which is capable of driving the assembly process to the prerequisite stacking. For instance, alkyl side chains with C_n = C_5H_{11}, C_8H_{17}, and $C_{13}H_{27}$ were incorporated to the perylenetetracarboxyldiimide ring to help inducing the self-assembly of PTCDIs into one-dimensional (1-D) nanowires depending on $\pi-\pi$ stacking via solution-phase self-assembly along the long wire direction.[17] The introduction of long alkoxy groups onto the aromatic core of conjugated-semiconductor molecule was found to be one of the effective ways in improving the OFET performance through improving the liquid crystal property of the corresponding organic semiconducting materials, which is beneficial in optimizing the $\pi-\pi$ stacking to fabricate well-ordered structure. In addition, solution processing method was also employed to optimize the molecular packing of 6,13-bis(triisopropylsilylethynyl) pentacene (TIPS-pentacene), inducing the decrease of the $\pi-\pi$ stacking distance from 3.33 to 3.08 Å, which in turn results in an increase in the hole mobility from 0.8 to 4.6 cm^2 V^{-1} s^{-1}.[18] The devices based on the self-assembled nanowires of poly(para-phenylene ethynylene) derivative with thioacetate end groups (TA-PPE) show the charge carrier mobility of 0.1 cm^2 V^{-1} s^{-1}, which is 3−4 orders higher than that of the thin film-based transistors of the same polymer.[19]

It is well-known that ambipolar semiconductors that allow dual operation of both *p*- and *n*-types have been highly desired for practical application in integrated circuits like high gain

Received: December 17, 2015
Accepted: February 19, 2016
Published: February 19, 2016

DOI: 10.1021/acsami.5b12368
ACS Appl. Mater. Interfaces 2016, 8, 6174−6182

complementary metal-oxide-semiconductor inverters and light emitting devices.[20−24] However, ambipolar counterparts still lag far behind the highly developed unipolar *p*-type and *n*-type organic semiconductors in terms of the low and unbalanced mobility for hole and electron, poor stability under ambient condition, low-solubility for solution processing, and large barrier against the injection of electron and/or hole carrier. Fortunately, the sandwich-type tetrapyrrole rare earth compounds with large conjugated macrocycle plane and extended network along the axis perpendicular to the macrocycle plane have been identified as promising ambipolar semiconducting molecular materials due to their solution processability and air stability.[8,25−28] As mentioned above, 1-D nanostructures have been clearly proved helpful in improving the performance of the unipolar *p*-type and *n*-type organic field-effect transistors;[29] however, OFETs that are based on the 1-D nanostructures of ambipolar organic semiconductors have not yet been well studied, to the best of our knowledge.[30] This is certainly true for sandwich-type tetrapyrrole rare earth compounds due to the difficulty in controlling the balance between the strong $\pi-\pi$ interaction among the macrocycle planes and the hydrophobic/hydrophilic interactions among the side chains linked at the macrocycle periphery.[31]

With these ideas in mind, herein we describe the design and synthesis of a novel amphiphilic mixed (phthalocyaninato) (porphyrinato) europium(III) triple-decker complex [Pc(OPh)$_8$]Eu[Pc(OPh)$_8$]Eu[TP(C≡CCOOH)PP] (**1**) [Pc(OPh)$_8$ = 2,3,9,10,16,17,23,24-octaphenoxyphthalocyaninate; TP(C≡CCOOH)PP = meso-[5-[4[(4-carboxylphenyl)-ethynyl] phenyl][10,15,20-tri[4-(octyloxy)phenyl]porphyrin]], Scheme 1. Electrochemical study reveals the potential ambipolar semiconducting nature of this compound, which is confirmed by the performance of the OFET devices fabricated by quasi-Langmuir-Shäfer (QLS) technique at the air/water interface with nanoparticle morphology with the hole and electron mobility of 7.0×10^{-7} and 7.5×10^{-7} cm^2 V^{-1} s^{-1}, respectively. However, the performance of the devices fabricated via a "phase-transfer" method from *n*-hexane with one-dimensional nanoribbon morphology was significantly improved by 3−6 orders of magnitude in terms of both hole and electron mobility, 0.11 and 4×10^{-4} cm^2 V^{-1} s^{-1}.

Scheme 1. Schematic Structure of Compound 1

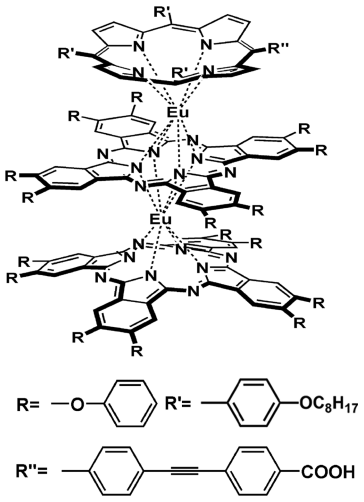

RESULTS AND DISCUSSION

Synthesis and Characterization of Compound 1. For the purpose of preparing amphiphilic mixed (phthalocyaninato) (porphyrinato) europium triple-decker complex with suitable HOMO and LUMO energy levels, one carboxyl group with electron-withdrawing nature as typical hydrophilic substituent was incorporated onto one of the four meso-attached phenyl moieties of the porphyrin ligand and eight phenoxyl substituents with weak electron-withdrawing ability as typical hydrophobic substituent was introduced onto the periphery of the phthalocyanine ligand. 5-(4-Iodophenyl)-10,15,20-tri-[4-octyloxy)phenyl] porphyrinato zinc was synthesized according to the published procedure,[32,33] which reacted with 4-ethynylbenzoate in the presence of $Pd(PPh_3)_2Cl_2$ and CuI in THF and Et_3N, affording Zn[TP(C≡CCOOCH$_3$)PP]. Treatment of Zn[TP(C≡CCOOCH$_3$)PP] with acetic acid led to the metal free porphyrin H_2TP(C≡CCOOCH$_3$)PP (**2**). Further reaction of H_2TP(C≡CCOOCH$_3$)PP with Eu[Pc(OPh)$_8$]$_2$ in the presence of [Eu(acac)$_3$]·*n*H$_2$O in TCB afforded the mixed (phthalocyaninato) (porphyrinato) europium triple-decker complex [Pc(OPh)$_8$]Eu[Pc(OPh)$_8$]Eu[TP(C≡CCOOCH$_3$)PP] (**3**), which was treated by several drops of NaOH (3 M) in refluxing THF, leading to the isolation of the target triple-decker compound with typical amphiphilic nature compound **1**. This newly prepared triple-decker compound was characterized by a series of spectroscopic techniques including MALDI-TOF and ^{1}H NMR spectra (Figures 1 and 2) as detailed in the experimental section.

Electrochemical Property of Compound 1. Cyclic voltammetry (CV) measurement of compound **1** in CH_2Cl_2 reveals a few quasi-reversible one-electron redox couples, with the first half-wave oxidation and first half-wave reduction potentials at +0.61 and -0.55 V (vs SCE), respectively, Figure 3. On the basis of electrochemical results and according to the literature method with the formula of $E_{HOMO} = -E_{1/2}^{oxd1} - 4.44$ eV and $E_{LUMO} = -E_{1/2}^{red1} - 4.44$ eV,[34] the HOMO and LUMO energy levels for this compound are therefore estimated to be −5.05 and −3.89 eV, respectively. These results suggest good match of this triple-decker compound with the Au electrodes.[35] In addition, its HOMO and LUMO energy levels facilitate both the hole and electron injection, ensuring the good *p*- and *n*-type organic semiconducting potential of this triple-decker compound in ambipolar OFET devices.

Fabrication and Morphology of the Self-Assembled Nanostructures. The very good solubility of the triple-decker complex in common organic solvents renders it possible to fabricate this compound into highly ordered supramolecular structures through solvent-based procedures. Due to the significant difference of **1** in chloroform (good solvent) and *n*-hexane (poor solvent), this compound was feasibly fabricated into corresponding nanostructures by means of the "phase-transfer" method, Scheme S1a (Supporting Information). The 1-D nanoribbons were fabricated by adding 3 mL of *n*-hexane to a 1 mL solution of compound **1** in chloroform (~1 mg/mL) to induce the precipitation and self-assembly at room temperature for 48 h. The quite different polarity between the chloroform and *n*-hexane provides the possibility to keep the two solvents in separate phases for an extended period. As a consequence, slow crystallization of **1** at the interface between chloroform and *n*-hexane, where slow "phase transfer" between the two solvents diminishes the solubility at the interface, resulting in the one-dimensional nanoribbons with the

DOI: 10.1021/acsami.5b12368
ACS Appl. Mater. Interfaces 2016, 8, 6174−6182

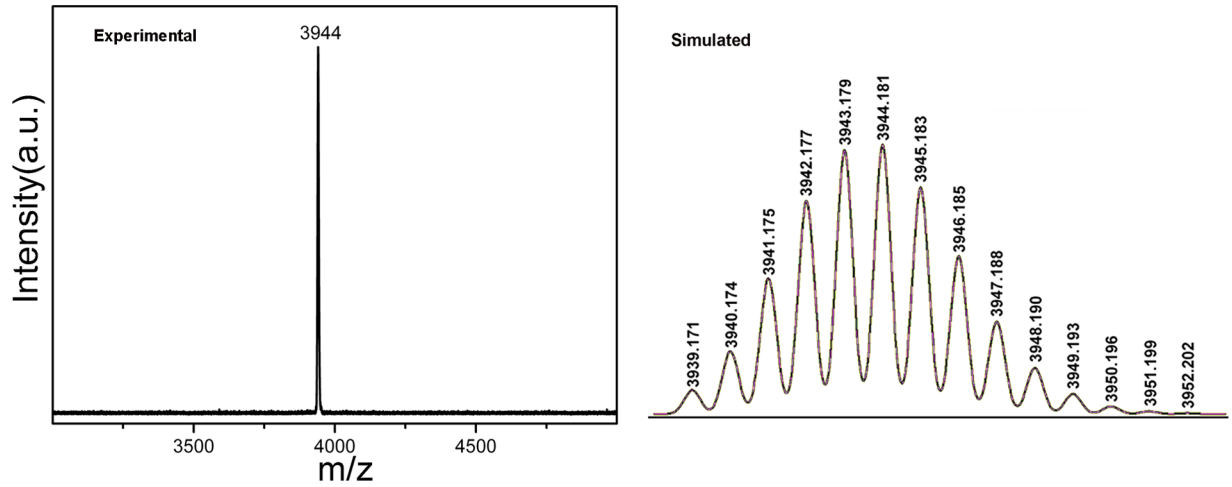

Figure 1. Experimental and simulated isotopic patterns for the molecular ion of compound **1** shown in the MALDI-TOF mass spectra.

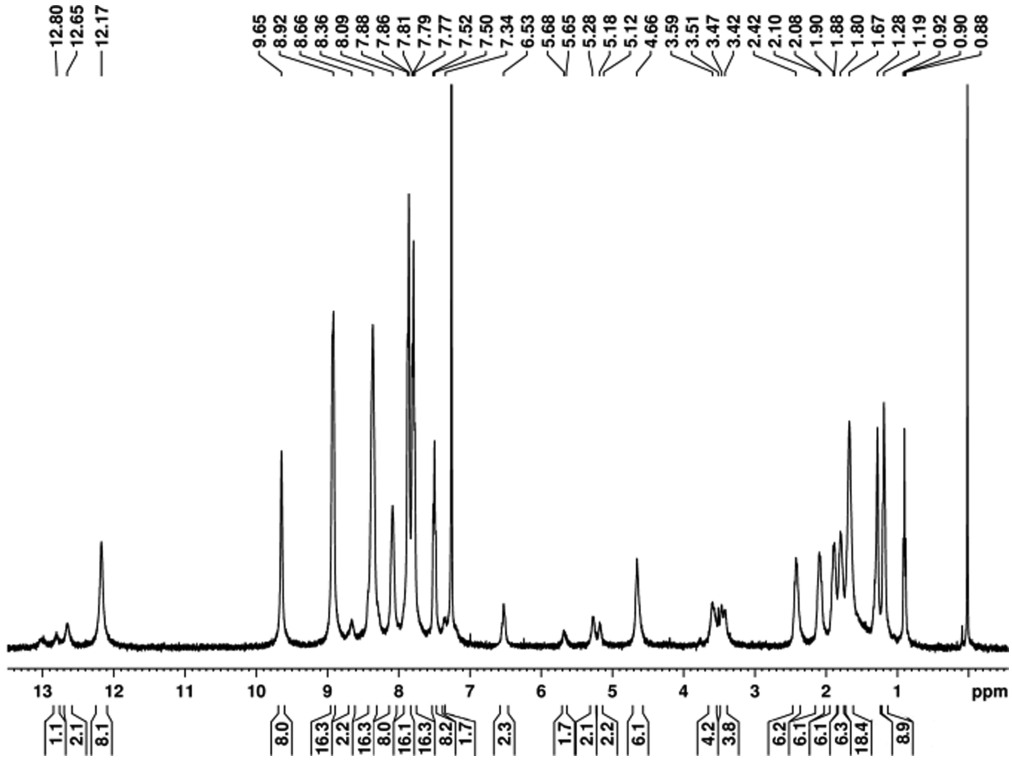

Figure 2. ^{1}H NMR spectrum of compound **1** in $CDCl_3$.

dimensions of a few tens of micrometers in length and about 120 ± 20 nm in width, Figure 4a,c, leading to an aspect ratio (length/width) in a magnitude of 100. The average thickness as measured by AFM amounts to ca. 60 nm, resulting in an aspect ratio of the ribbon cross-section (width/thickness) around 2:1, which is approximately consistent with the unit-cell parameter consisting of a dimeric supramolecular structure according to the energy-optimized molecular structure and XRD analysis (vide infra), for which the ratio of the longitudinal edge-to-edge distance between two adjacent triple-decker molecules and transverse distance of a supramolecular dimeric building block is close to 2:1 (3.40/1.69), Figures 5 and S1 (Supporting Information). On the other hand, considering the typical amphiphilic nature of this novel triple-decker compound, the QLS method was also employed to prepare the nanostructures for **1** according the published procedure.[36] A chloroform solution of **1** was injected into the center of a cylindrical glass container, and then water was carefully added onto the surface of the chloroform solution until 90% of the surface was covered by water, leaving only a small hole for the evaporation of the organic solvent. After the complete evaporation of $CHCl_3$, triple-decker molecules gradually assembled to form some fine nanostructures on the water surface, which can be easily transferred from the water surface onto a glass or SiO_2/Si substrate by horizontal lifting, resulting in the QLS film of **1**, Scheme S1b (Supporting Information). AFM observation clearly indicates the film morphology which consisting of the uniformed nanoparticles with approximately 200−230 nm in diameter, giving a root-mean-square (Rrms) roughness value of 2.93 nm, Figure 4b. Such a typical particularly smooth surface

DOI: 10.1021/acsami.5b12368
ACS Appl. Mater. Interfaces 2016, 8, 6174−6182

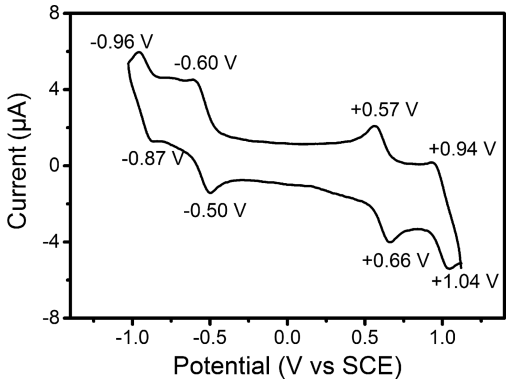

Figure 3. Cyclic voltammogram (CV) of compound **1** at a scan rate of 20 mV s^{-1}.

film-structure was further confirmed by SEM observation, Figure 4d. The granular morphology of the QLS film of **1** is consistent with the weaker $\pi-\pi$ stacking as well revealed by the electronic absorption spectroscopic result detailed below, which in turn prevents the molecules from assembling along one particular dimension. However, the favorable $\pi-\pi$ stacking of the dimeric supramolecular structures (formed through the intermolecular hydrogen bonds between the triple-decker molecules confirmed by XRD and FT-IR) (vide infra) leads to the formation of one-dimensional (1-D) molecular assembly, actually the nanoribbons of **1**, realized by using the phase-transfer self-assembly from a concentrated chloroform solution to excess amount of *n*-hexane.[17]

To further reveal the difference in the internal structure between nanoribbons and nanoparticles, their morphology was examined by a high-revolution transmission electron microscope (HRTEM), Figure 4e,f. The lattice fringe was clearly observed for the nanoribbons, indicating the excellent crystallinity of the ribbons. The result is indexed quite well with the lattice parameter of 1.69 nm obtained from XRD data as detailed below. However, lattice fringe was not observed for the QLS film of **1**, confirming the poor crystallinity nature of the QLS film.

X-ray Diffraction Patterns. The internal structures of the nanoribbons and QLS film nanoparticles were investigated by XRD analysis. As shown in Figure 5a, in the low angle range, the XRD diagram of the nanoribbons formed from *n*-hexane shows two clear diffraction peak at $2\theta = 4.10°$ (2.15 nm) and $2\theta = 5.24°$ (1.69 nm), which are ascribed to the diffractions from the (001) and (100) planes, respectively, related to the distances between triple-decker columns, Figure 5c, based on the energy-optimized triple-decker molecular structure obtained using PCMODEL for windows Version 6.0, Serena Software, Figure S1 (Supporting Information).[32] Furthermore, the XRD pattern also exhibits three weaker high order diffractions at 1.03, 0.70, and 0.43 nm, which are attributed to the diffractions from the (002), (003), and (005) planes, respectively, indicating the existence of regular repeating unit (actually good molecular ordering) in the nanostructure along the *c*-axis of the unit cell (or the direction perpendicular to the tetarpyrrole rings). It is noteworthy that additional diffractions at 0.32 and 0.27 nm were present in the wide angle region of the XRD pattern of nanoribbons. The former of which can be attributed to the $\pi-\pi$ stacking distance between tetrapyrrole cores of neighboring triple-decker molecules, while the later one to the intermolecular hydrogen bond length in the dimeric supramolecular structure of the nanoribbons,[32] in line with the IR spectroscopic result as detailed below. It is worth mentioning that the good molecular ordering, i.e. the intensive intra/intermolecular $\pi-\pi$ interactions, along the direction perpendicular to the tetrapyrrole rings revealed is certainly expected to contribute to the remarkable carrier mobility for the transistor devices fabricated from the nanoribbons as detailed below. In contrast, the XRD diagram of the QLS film of **1** shows only one peak at 2.67 nm in the low angle range, corresponding to a periodic distance between two adjacent triple-decker molecules, Figure 5b. Judging from the diagonal dimension of the compound **1** molecule obtained on the basis

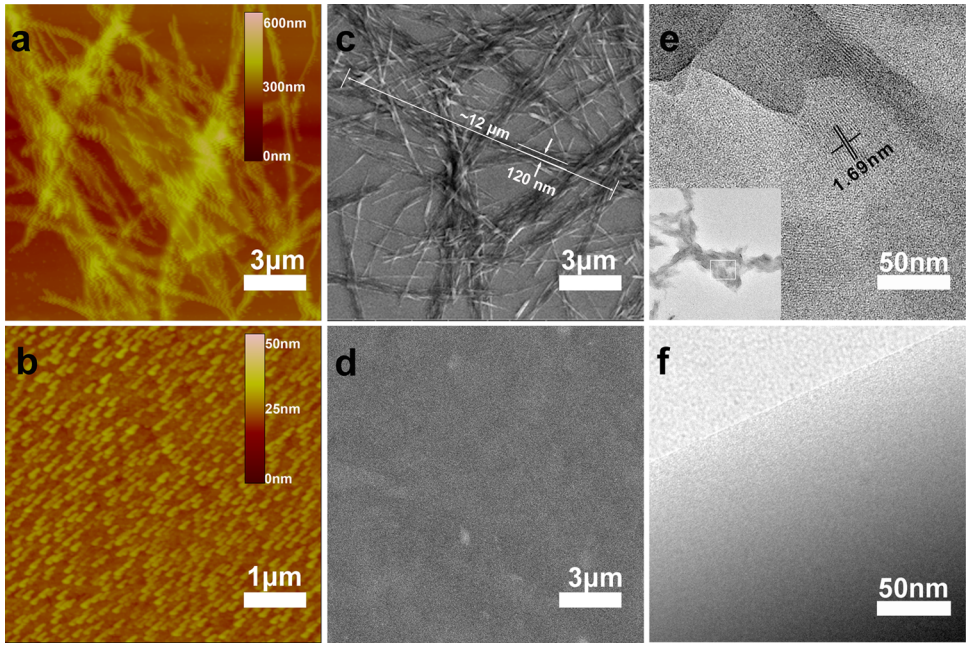

Figure 4. AFM, SEM, and TEM images of the nanoribbons (a, c, and e) and QLS film (b, d, and f) of **1**.

DOI: 10.1021/acsami.5b12368
ACS Appl. Mater. Interfaces 2016, 8, 6174−6182

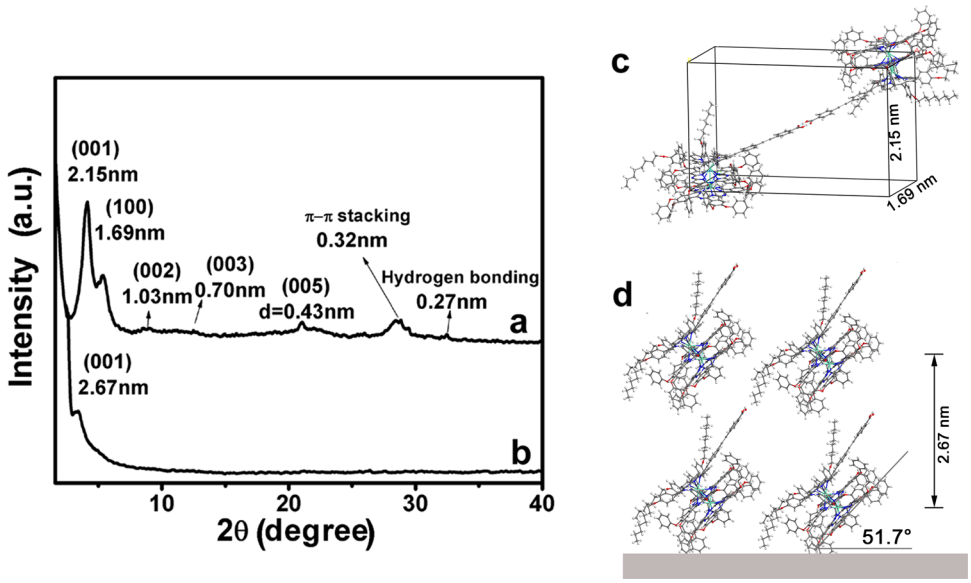

Figure 5. XRD patterns of the nanoribbons (a); the QLS film (b); and the schematic representation of the unit cell in the nanoribbons (c) and of the packing mode in the QLS film (d) of **1**.

of the energy-optimized molecular structure, 3.40 nm, the orientation angle between the tetrapyrrole ring in the triple-decker molecule and substrate surface is calculated to amount to ca. 51.7°. This result is in good accordance with that deduced from UV−vis spectroscopic measurement, revealing the employment of an edge-on orientation by the triple-decker molecules with the tetrapyrrole rings tilted to the substrate surface, Figure 5d. In addition, unlike the nanoribbons no diffraction peak related to the triple-decker intermolecular hydrogen bond was detected for the QLS film, due to the formation of the hydrogen bond between the triple-decker molecule and the water solvent molecules at the air/water interface. At the end of this section, it is worth noting that observation of the significantly increased intensity and sharpness for the diffraction peaks in the low-angle region for nanoribbons than those of the QLS film of the same triple-decker clearly manifests the obviously improved molecular packing ordering and heightened crystallinity in the nanoribbons over the QLS film nanoparticles.

Electronic Absorption Spectra. Figure 6 compares the electronic absorption spectra of compound **1** in $CHCl_3$, the nanoribbons self-assembled from *n*-hexane, and nanoparticles fabricated by the QLS method. As can be seen, the compound in $CHCl_3$ shows a typical feature of the electronic absorption spectrum for mixed (phthalocyaninato) (porphyrinato) rare earth triple-decker complexes,[25,26,37] revealing the nonaggregated molecular spectroscopic nature of this compound when being dissolved in $CHCl_3$. The intense and sharp absorptions around 358 and 418 nm can be attributed to the phthalocyanine and porphyrin Soret bands of triple-decker compound, respectively, while the three relatively weak absorptions at 555, 635, and 726 nm to their Q bands with contribution from both species of tetrapyrrole chromophores but dominated by phthalocyanine due to its much more intensive absorptions than those of porphyrin in this area. As clearly shown in Figure 6, in comparison with the spectrum of chloroform solution, the porphyrin Soret band for the nanoribbons of **1** revealed a red-shift from 418 to 422 nm. However, the phthalocyanine Soret band takes a significant blue shift from 358 to 352 nm. Actually, all the three Q absorption bands also blue-shifted from 555, 635, and 726 nm to 532, 623, and 718 nm, respectively. Interestingly, this occurs again when the same triple-decker was fabricated into the nanoparticles by QLS technique but with a diminished degree of shift for all the corresponding absorption bands, Figure 6, as exemplified by the most intense Q-band of the QLS nanoparticles blue-shifted by 16 nm (from 555 to 539 nm) versus that of nanoribbons, 23 nm (from 555 to 532 nm). This is truly strange since the thus far investigations have revealed that mixed (phthalocyaninato) (porphyrinato) rare earth double/triple-deckers usually act as a whole molecular building block to participate in the self-assembly process due to the intensive intramolecular $\pi-\pi$ interaction(s), resulting in the simultaneous shift of all the absorption bands of the tetrapyrrole sandwich compounds to either lower or higher energy direction depending on the head-to-tail (*J*-aggregate) and parallel (*H*-aggregate) molecular packing in the nanostructures, respectively.[38−42] However, the present phenomenon is in line with those found for some aggregates formed from planar conjugated systems including phthalocyanine,[43] porphyrin,[44] and perylenetetracarboxylic diimide derivatives,[45] in which the dipoles of the molecules are considered to be arranged in an

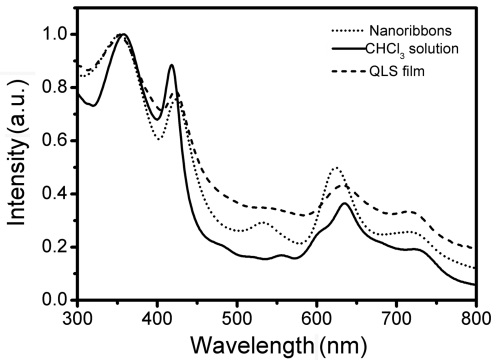

Figure 6. Electronic absorption spectra of compound **1** in chloroform solution (solid line), the nanoribbons dispersed in *n*-hexane (dot line) and the QLS film of **1** (dash line).

DOI: 10.1021/acsami.5b12368
ACS Appl. Mater. Interfaces 2016, 8, 6174−6182

intermediate case between typical head-to-tail (*J*-aggregate) and parallel (*H*-aggregate) arrangements according to the exciton theory.[46] In other words, the macrocyclic planes of the conjugated planar molecules take either a "face-to-face" conformation or a "edge-on" orientation in their aggregates. This seems also true for the present case. Actually, due to the typical amphiphilic nature of **1**, during the self-assembly procedure using QLS method, the triple-decker molecule most probably adopts the edge-on orientation with hydrophilic carboxyl groups adjacent to the water surface and the hydrophobic phthalocyanine rings obliged toward the air phase at the air/water interface, Figure 5 and Scheme S1b (Supporting Information), resulting in the isolation of the QLS film with nanoparticle morphology with the same molecular arrangement.[11] However, it is worth noting that during the self-assembly process of **1** in chloroform and *n*-hexane by a "phase transfer" method, at the very beginning a dimeric supramolecule structure was bridged first through two hydrogen bonds formed between the carboxyl group of two triple-decker molecules, which as the basic building block further self-assembles into nanoribbons in which the tetrapyrrole chromophores for the adjacent dimers employ a face-to-face conformation depending mainly on the $\pi-\pi$ stacking with the help of van der Waals interactions, Figure 5. Further support for this point comes clearly from the FT-IR spectroscopic results as detailed below.

FT-IR Spectra. In order to evaluate the contribution of the carboxyl group conformation and packing to the internal structures of the nanostructures of **1**, IR spectroscopic measurements were carried out. Figure 7 displays the IR

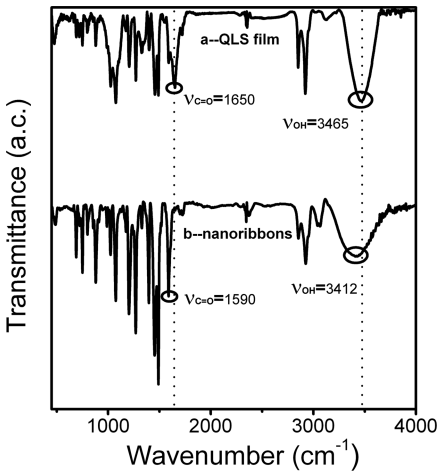

Figure 7. IR spectra of QLS film (a) and nanoribbons (b) in the region 400−4000 cm^{-1}.

spectra of self-assembled nanostructures including the nanoribbons and QLS film nanoparticles. As can be seen, an intense band appearing at approximately 1650 cm^{-1} in the QLS film due to the $\nu_{C=O}$ stretching vibration of the carboxyl group from the triple-decker **1** red-shifts to a lower frequency of 1590 cm^{-1} in the IR spectrum of the nanoribbons due to the formation of the dimeric supramolecular structure depending on the intermolecular hydrogen bond between carboxyl groups of the neighboring triple-decker molecules in the nanoribbons on the basis of previous studies.[32,47−49] This is further supported by the observation of a new intensive band at 3412 cm^{-1} in the IR spectrum of the nanoribbons of **1**, which is attributed to the hydrogen bonding stretching vibration. It is, however, noteworthy that the strong band appearing at 3465 cm^{-1} in the QLS film is also due to the stretching vibration of hydrogen bond formed between the triple-decker carboxyl groups with water instead of another carboxyl group of the neighboring triple-decker molecule during the fabrication procedure using QLS technique associated with the strong hydrophility of carboxyl group. These results are also in line with the X-ray diffraction (XRD) analyses.

OFET Properties. For the purpose of investigating the semiconducting property of the present triple-decker compound, OFET devices were fabricated from both nanoribbons and QLS film (nanoparticles) of **1** by employing the typical top-contact/bottom-gate configuration with the vacuum-deposited source and drain electrodes on the top of the nanoribbons and the QLS film, respectively. As exemplified in Figures 8 and 9, the devices fabricated from both nanostructures showed typical ambipolar (both *p*- and *n*-type) characteristics under ambient conditions, confirming the ambipolar semiconducting nature of this compound as predicted according to its electrochemical property. The QLS film revealed the quite low carrier mobilities with the values of 7.0 × 10^{-7} and 7.5 × 10^{-7} cm^2 V^{-1} s^{-1} for hole and electron, respectively, and the on/off ratios of 10^2 for both electron and hole, Figure 8 and Table S1 (Supporting Information). However, the 1-D nanoribbons-based OFET devices display significantly improved performance with the carrier mobilities for hole and electron, up to 0.11 and 4 × 10^{-4} cm^2 V^{-1} s^{-1}, respectively, Figure 9 and Table S1 (Supporting Information), and the on/off ratios of 10^6 for hole and 10^4 for electron.

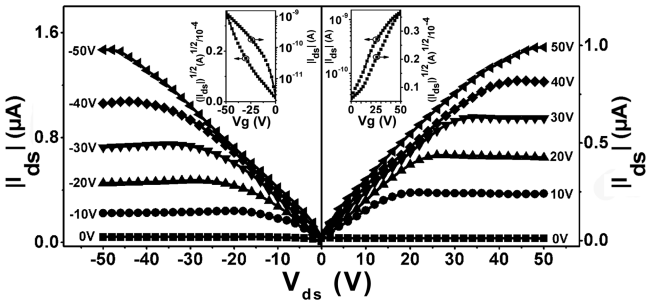

Figure 8. Output characteristics (I_{ds} versus V_{ds}) and (insets) transfer characteristics ($|I_{ds}|^{1/2}$ versus V_g) for the ambipolar OFET device based on QLS film of compound **1** deposited on SiO_2/Si (300 nm) substrate with Au top contact measured in air.

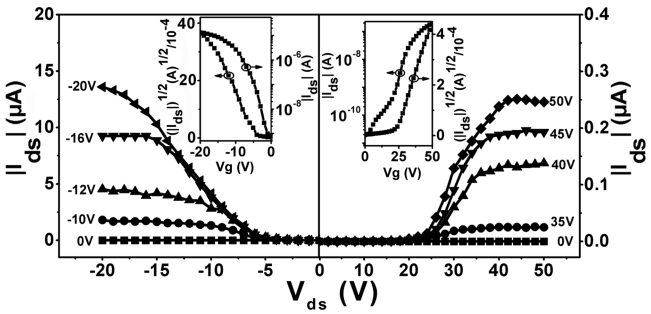

Figure 9. Output characteristics (I_{ds} versus V_{ds}) and (insets) transfer characteristics ($|I_{ds}|^{1/2}$ versus V_g) for the ambipolar OFET device based on 1-D nanoribbons deposited on SiO_2/Si (300 nm) substrate with Au top contact measured in air.

DOI: 10.1021/acsami.5b12368
ACS Appl. Mater. Interfaces 2016, 8, 6174−6182

Among the totally examined 20 devices, over 50% devices display the average value for electron of $(4 \pm 0.8) \times 10^{-4}$ cm^2 V^{-1} s^{-1} and for hole of 0.11 ± 0.05 cm^2 V^{-1} s^{-1}, respectively, Figure S2 (Supporting Information). Obviously, the more denser $\pi-\pi$ stacking and higher ordering of molecules in combination with the increased crystallinity for nanoribbons relative to those of the QLS films enhance the orbital overlap and thereby facilitate charge carrier transport between electrodes to semiconductor materials in the OFET devices.[50] In addition, the decrease of the operating voltage range from 0 ~ −50 V for QLS film-based OFETs to 0 ~ −20 V for the nanoribbons-based devices further indicated the effectiveness of the molecular alignment and ordering on the device behavior. Nevertheless, the threshold voltages (V_{th}) also change from the QLS film-based device (−8 and +8 V for hole and electron) to −3 V for hole and +17 V for electron for the nanoribbons. The increase of V_{th} for electron from QLS film to nanoribbons could be ascribed to the significant contact resistance due to the nonideal semiconductor−metal interface.[51] It is worth noting that despite the value of HOMO level (−5.05 eV) of compound **1** is nearly identical to the Fermi level of the Au electrode (−5.1 eV), the contact effect still exists in the linear region for both the electron and the hole transport. Actually, in addition to the Mott−Schottky barrier for the carrier (hole and electron) injection, the charge carrier trap states within the nanoribbons and the organic semiconductor−metal interface can also lead to the contact effect.[52] Only after the deep traps are filled, the charge can be migrated. In other words, a higher gate voltage has to be applied to overcome the threshold voltage (V_{th}). However, it is worth noting that the transfer and output characteristics of the saturation regime for the 1-D nanoribbons have not been affected by the contact resistance since the gate electric field applied will induce the charge to fill the traps and overcome the contact resistance, which in turn helps the hole and electron injection into the organic semiconducting layer from the gold electrodes. More importantly, the device performance was found to remain stable in terms of both the carrier mobilities and on/off ratios even after being put in air for more than two months.

At the end of this section, it is worth noting that the LUMO energy level of an air-stable *n*-type semiconductor normally should below −4.0 eV to against the air-derived electron traps.[53,54] However, in the present case the LUMO energy level of **1**, −3.89 eV, actually does not meet this request. The unexpected air stability of this compound in both the QLS film-based and the nanoribbons-based OFET devices is therefore attributed to the molecular packing mode in the QLS film and the nanoribbons.[50,54,55] Most probably, the densely packed tetrapyrrole cores together with the closely packed phenoxy substituents and alkoxyl chains provide a kinetic barrier to the diffusion of oxygen and moisture into the channel region in the devices.[54]

CONCLUSION

Briefly summarizing above, combination of molecular design and a solution-based phase-transfer self-assembly led to the successful fabrication of OFET devices from a novel amphiphilic mixed (phthalocyaninato) (porphyrinato) europium(III) triple-decker complex with crystalline 1-D nanoribbon morphology, exhibiting air-stable ambipolar semiconducting performance with hole and electron mobilities of 0.11 and 4×10^{-4} cm^2 V^{-1} s^{-1}, respectively, 3−6 orders higher than those of thin film transistors made by the QLS method. The formation of a dimeric supramolecular structure on account of the intermolecular hydrogen bonding between two triple-decker molecules was revealed to minimize the steric hindrance for the basic building blocks organized along the direction perpendicular to the tetrapyrrole rings into the one-dimensional nanoribbons depending on the increased $\pi-\pi$ stacking interaction with the help of van der Waals force. This in turn becomes responsible for the significantly improved device performance over the transistors based on QLS film with nanoparticle morphology and lack of intermolecular hydrogen bonding-based dimeric supramolecular structure building block. It is worth noting that the present result, actually representing the first OFET device based on the 1-D small molecular-based nanostructures with air-stable ambipolar device performance, will surely contribute to the future development of small molecular-based organic electronics with potential application in nanoelectronic and optoelectronics complementary integrated circuits by means of molecular design and fabrication technique.

EXPERIMENTAL SECTION

Synthesis of Meso-[5-[4[(4-carboxylphenyl)ethynyl]phenyl]-[10,15,20-tri[4-(octyloxy) phenyl]]porphyrin H_2TP(C≡CCOOCH$_3$)PP (2). Compound **2** was prepared by 5-(4-iodophenyl)-10,15,20,-tri-[4-(octyloxy)phenyl] porphyrinato zinc and methyl-4-ethynylbenzoate in the presence of $Pd(PPh_3)_2Cl_2$ and CuI in THF and Et_3N, in detail please see the Supporting Information. ^{1}H NMR (400 MHz, $CDCl_3$, δ): 8.89 (d, 6 H, Por-Ph-H), 8.82 (d, 2 H, Por-Ph-H), 8.22 (d, 2 H, Por-Ph-H), 8.11 (d, 8 H, Por-*β*-H), 7.93 (d, 2 H, Por-Ph-H), 7.73 (d, 2 H, Por-Ph-H), 7.28 (s, 6 H, Por-Ph-H), 4.26−0.93 (m, 51 H, Por-Ph-OC_8H_{17}), 3.97 (s, 3 H, $COOCH_3$−H), - 2.78 (s, 2 H, N−H), Figure S3 (Supporting Information). MALDI-TOF MS: an isotopic cluster peaking at m/z 1158, Calcd for $C_{78}H_{84}N_4O_5$, $[M]^+$, 1158, Figure S4 (Supporting Information). Anal. Calc. For $C_{78}H_{84}N_4O_5$: C, 80.9%; H, 7.31%; N, 4.84%. Found: C, 80.8%; H, 7.07%; N, 4.85%.

Synthesis of [Pc(OPh)$_8$]Eu[Pc(OPh)$_8$]Eu[TP(C≡CCOOCH$_3$)PP] (3). Compound **3** was prepared from a mixture of compound **2**, $Eu[Pc(OPh)_8]_2$, and $Eu(acac)_3{\cdot}nH_2O$ in TCB following the procedure reported previously by ourselves,[32] in detail please see the Supporting Information. MALDI-TOF MS: an isotopic cluster peaking at m/z 3956, Calc. for $C_{238}H_{178}Eu_2N_{20}O_2$, $[M]^+$, 3956, Figure S5 (Supporting Information). Anal. Calcd For $C_{238}H_{178}Eu_2N_{20}O_2$: C, 72.2%; H, 4.53%; N, 7.08%. Found: C, 72.9%; H, 4.51%; N, 7.07%.

Synthesis of Compound 1. Compound **1** was prepared by hydrolyzing THF, and then several drops of 3 M NaOH were added. The mixture was refluxed overnight. The solvent was removed under reduced pressure and the residue left was chromatographed on a silica gel column with $CHCl_3$ as eluent. ^{1}H NMR (400 MHz, $CDCl_3$, δ): 12.17 (s, 8 H, Pc-H*α*), 9.65 (s, 8 H, Pc*-H*α*), 8.92 (d, 16 H, Pc-Ph-Ho), 8.36 (t, 16 H, Pc-Ph-Hm), 8.09 (t, 8 H, Pc-Ph-Hp), 7.88 (d, 16 H, Pc*-Ph-Ho), 7.79 (t, 16 H, Pc*-Ph-Hm), 7.52 (t, 8 H, Pc*-Ph-Hp), 12.65, 8.66, 7.50, 6.53 (s, 8 H, Por-*β*-H), 5.68−3.42 (m, 20 H, Por-Ph-H), 2.42−1.19 (m, 51 H, Por-Ph-OC_8H_{17}). MALDI-TOF MS: an isotopic cluster peaking at m/z 3944, Calcd for $C_{237}H_{176}Eu_2N_{20}O_2$, $[M]^+$, 3944. Anal. Calc. For $C_{237}H_{176}Eu_2N_{20}O_2$: C, 72.17%; H, 4.50%; N, 7.10%. Found: C, 72.6%; H, 4.63%; N, 7.06%.

ASSOCIATED CONTENT

Supporting Information

The Supporting Information is available free of charge on the ACS Publications website at DOI: 10.1021/acsami.5b12368.

Additional characterization and experimental data including structural characterization data, OFET data for compound **1** and details of synthesis and character-

DOI: 10.1021/acsami.5b12368
ACS Appl. Mater. Interfaces 2016, 8, 6174−6182

izations for compounds **2** and **3**. The preparation procedure and schematic diagram of device. (PDF)

AUTHOR INFORMATION

Corresponding Authors

*E-mail: yanlichen@upc.edu.cn.

*E-mail: jianzhuang@ustb.edu.cn.

Notes

The authors declare no competing financial interest.

ACKNOWLEDGMENTS

This work was financially supported by the National Key Basic Research Program of China (Nos. 2013CB933402 and 2012CB224801) and the National Natural Science Foundation of China (Nos. 21290174, 21371073, and 21401009).

REFERENCES

(1) Dimitrakopoulos, C. D.; Malenfant, P. R. L. Organic Thin Film Transistors for Large Area Electronics. *Adv. Mater.* **2002**, *14* (2), 99−117.

(2) Li, R.; Hu, W.; Liu, Y.; Zhu, D. Micro- and Nanocrystals of Organic Semiconductors. *Acc. Chem. Res.* **2010**, *43* (4), 529−540.

(3) Usta, H.; Facchetti, A.; Marks, T. J. n-Channel Semiconductor Materials Design for Organic Complementary Circuits. *Acc. Chem. Res.* **2011**, *44* (7), 501−510.

(4) Wu, W.; Liu, Y.; Zhu, D. π-Conjugated Molecules with Fused Rings for Organic Field-Effect Transistors: Design, Synthesis and Applications. *Chem. Soc. Rev.* **2010**, *39* (5), 1489−1502.

(5) Ortiz, R. P.; Facchetti, A.; Marks, T. J. High-*k* Organic, Inorganic, and Hybrid Dielectrics for Low-Voltage Organic Field-Effect Transistors. *Chem. Rev.* **2010**, *110* (1), 205−239.

(6) Liu, S.; Wang, W. M.; Briseno, A. L.; Mannsfeld, S. C. B.; Bao, Z. Controlled Deposition of Crystalline Organic Semiconductors for Field-Effect-Transistor Applications. *Adv. Mater.* **2009**, *21* (12), 1217−1232.

(7) Wang, Y.; Chen, Y.; Li, R.; Wang, S.; Su, W.; Ma, P.; Wasielewski, M. R.; Li, X.; Jiang, J. Amphiphilic Perylenetretracarboxyl Diimide Dimer and Its Application in Field Effect Transistor. *Langmuir* **2007**, *23* (10), 5836−5842.

(8) Kan, J.; Chen, Y.; Qi, D.; Liu, Y.; Jiang, J. High-Performance Air-Stable Ambipolar Organic Field-Effect Transistor Based on Tris-(phthalocyaninato) Europium (III). *Adv. Mater.* **2012**, *24* (13), 1755−1758.

(9) Kong, X.; Zhang, X.; Gao, D.; Qi, D.; Chen, Y.; Jiang, J. Air-Stable Ambipolar Field-Effect Transistor Based on a Solution-Processed Octanaphthoxy-Substituted Tris(phthalocyaninato) Europium Semiconductor with High and Balanced Carrier Mobilities. *Chem. Sci.* **2015**, *6* (3), 1967−1972.

(10) Chen, Y.; Li, D.; Yuan, N.; Gao, J.; Gu, R.; Lu, G.; Bouvet, M. Tuning The Semiconducting Nature of Bis(phthalocyaninato) Holmium Complexes via Peripheral Substituents. *J. Mater. Chem.* **2012**, *22* (41), 22142−22149.

(11) Chen, Y.; Su, W.; Bai, M.; Jiang, J.; Li, X.; Liu, Y.; Wang, L.; Wang, S. High Performance Organic Field-Effect Transistors Based on Amphiphilic Tris(phthalocyaninato) Rare Earth Triple-Decker Complexes. *J. Am. Chem. Soc.* **2005**, *127* (45), 15700−15701.

(12) Bendikov, M.; Wudl, F. Tetrathiafulvalenes, Oligoacenenes, and Their Buckminsterfullerene Derivatives: The Brick and Mortar of Organic Electronics. *Chem. Rev.* **2004**, *104* (11), 4891−4946.

(13) Hutchison, G. R.; Ratner, M. A.; Marks, T. J. Intermolecular Charge Transfer between Heterocyclic Oligomers. Effects of Heteroatom and Molecular Packing on Hopping Transport in Organic Semiconductors. *J. Am. Chem. Soc.* **2005**, *127* (48), 16866−16881.

(14) Halik, M.; Klauk, H.; Zschieschang, U.; Schmid, G.; Ponomarenko, S.; Kirchmeyer, S.; Weber, W. Relationship between Molecular Structure and Electrical Performance of Oligothiophene Organic Thin Film Transistors. *Adv. Mater.* **2003**, *15* (11), 917−922.

(15) Facchetti, A.; Yoon, M.; Stern, C. L.; Katz, H. E.; Marks, T. J. Building Blocks for n-Type Organic Electronics: Regiochemically Modulated Inversion of Majority Carrier Sign in Perfluoroarene-Modified Polythiophene Semiconductors. *Angew. Chem., Int. Ed.* **2003**, *42* (33), 3900−3903.

(16) Miao, Q.; Lefenfeld, M.; Nguyen, T.; Siegrist, T.; Kloc, C.; Nuckolls, C. Self-Assembly and Electronics of Dipolar Linear Acenes. *Adv. Mater.* **2005**, *17* (4), 407−412.

(17) Briseno, A. L.; Mannsfeld, S. C. B.; Hancock, J. M.; Xiong, Y.; Jenekhe, S. A.; Bao, Z.; Xia, Y. Perylenediimide Nanowires and Their Use in Fabricating Field-Effect Transistors and Complementary Inverters. *Nano Lett.* **2007**, *7* (9), 2847−2853.

(18) Giri, G.; Verploegen, E.; Mannsfeld, S. C. B.; Atahan-Evrenk, S.; Kim, D. H.; Lee, S. Y.; Becerril, H. A.; Aspuru-Guzik, A.; Toney, M. F.; Bao, Z. Tuning Charge Transport in Solution-Sheared Organic Semiconductors Using Lattice Strain. *Nature* **2011**, *480* (7378), 504−508.

(19) Dong, H.; Jiang, S.; Jiang, L.; Liu, Y.; Li, H.; Hu, W.; Wang, E.; Yan, S.; Wei, Z.; Xu, W.; Gong, X. Nanowire Crystals of a Rigid Rod Conjugated Polymer. *J. Am. Chem. Soc.* **2009**, *131* (47), 17315−17320.

(20) Chua, L. L.; Zaumseil, J.; Chang, J.-F.; Ou, E.C.-W.; Ho, P.K.-H.; Sirringhaus, H.; Friend, R. H. General Observation of n-Type Field-effect Behaviour in Organic Semiconductors. *Nature* **2005**, *434* (7030), 194−197.

(21) Kim, F. S.; Ahmed, E.; Subramaniyan, S.; Jenekhe, S. A. Air-Stable Ambipolar Field-Effect Transistors and Complementary Logic Circuits from Solution-Processed n/p Polymer Heterojunctions. *ACS Appl. Mater. Interfaces* **2010**, *2* (11), 2974−2977.

(22) Walzer, K.; Maennig, B.; Pfeiffer, M.; Leo, K. Highly Efficient Organic Devices Based on Electrically Doped Transport Layers. *Chem. Rev.* **2007**, *107* (4), 1233−1271.

(23) Baldo, M. A.; Thompson, M. E.; Forrest, S. R. High-Efficiency Fluorescent Organic Light-Emitting Devices Using a Phosphorescent Sensitizer. *Nature* **2000**, *403* (6771), 750−753.

(24) Baldo, M. A.; O'Brien, D. F.; You, Y.; Shoustikov, A.; Sibley, S.; Thompson, M. E.; Forrest, S. R. Highly Efficient Phosphorescent Emission from Organic Electroluminescent Devices. *Nature* **1998**, *395* (6698), 151−154.

(25) Gao, D.; Zhang, X.; Kong, X.; Chen, Y.; Jiang, J. (TFPP)Eu-[$Pc(OPh)_8$]Eu[$Pc(OPh)_8$]/CuPc Two-Component Bilayer Heterojunction-Based Organic Transistors with High Ambipolar Performance. *ACS Appl. Mater. Interfaces* **2015**, *7* (4), 2486−2493.

(26) Zhang, X.; Chen, Y. A Sandwich Mixed(phthalocyaninato)(porphyrinato) Europium Triple-Decker: Balanced-Mobility, Ambipolar Organic Thin-Film Transistor. *Inorg. Chem. Commun.* **2014**, *39*, 79−82.

(27) Li, D.; Wang, H.; Kan, J.; Lu, W.; Chen, Y.; Jiang, J. H-aggregation Mode in Triple-Decker Phthalocyaninato-Europium Semiconductors. Materials Design for High-Performance Air-Stable Ambipolar Organic Thin Film Transistors. *Org. Electron.* **2013**, *14* (10), 2582−2589.

(28) Kong, X.; Jia, Q.; Wu, F.; Chen, Y. Flexible, Ambipolar Organic Field-Effect Transistors Based on The Solution-Processed Films of Octanaphthoxy-Substituted Bis(phthalocyaninato) Europium. *Dyes Pigm.* **2015**, *115*, 67−72.

(29) Elemans, J. A. A. W.; van Hameren, R.; Nolte, R. J. M.; Rowan, A. E. Molecular Materials by Self-Assembly of Porphyrins, Phthalocyanines, and Perylenes. *Adv. Mater.* **2006**, *18* (10), 1251−1226.

(30) Balakrishnan, K.; Datar, A.; Naddo, T.; Huang, J.; Oitker, R.; Yen, M.; Zhao, J.; Zang, L. Effect of Side-Chain Substituents on Self-Assembly of Perylene Diimide Molecules: Morphology Control. *J. Am. Chem. Soc.* **2006**, *128* (26), 7390−7398.

(31) Zhang, X.; Wang, Q.; Wu, L.; Lv, W.; Lu, J.; Bian, Y.; Jiang, J. Organic Nanostructures with Controllable Morphology Fabricated from Mixed (Phthalocyaninato) (porphyrinato) Europium Double-Decker Complexes. *J. Phys. Chem. B* **2010**, *114* (3), 1233−1240.

(32) Lu, G.; Chen, Y.; Zhang, X.; Bao, M.; Bian, Y.; Li, X.; Jiang, J. Morphology Controlled Self-Assembled Nanostructures of Sandwich

DOI: 10.1021/acsami.5b12368
ACS Appl. Mater. Interfaces 2016, 8, 6174−6182

Mixed (Phthalocyaninato) (Porphyrinato) Europium Triple-Deckers. Effect of Hydrogen Bonding on Tuning The Intermolecular Interaction. *J. Am. Chem. Soc.* **2008**, *130* (35), 11623−11630.
(33) Gao, Y.; Zhang, X.; Ma, C.; Li, X.; Jiang, J. Morphology-Controlled Self-Assembled Nanostructures of 5,15-Di[4-(5-acetylsulfanylpentyloxy)phenyl]porphyrin Derivatives. Effect of Metal-Ligand Coordination Bonding on Tuning The Intermolecular Interaction. *J. Am. Chem. Soc.* **2008**, *130* (50), 17044−17052.
(34) SCE energy level is taken to be −4.44 eV below the vacuum level, for detail please see: Bard, A. J.; Faulkner, L. R. *Electrochemical Methods-Fundamentals and Applications*; Wiley: New York, 1984.
(35) Zaumseil, J.; Sirringhaus, H. Electron and Ambipolar Transport in Organic Field-Effect Transistors. *Chem. Rev.* **2007**, *107* (4), 1296−1323.
(36) Chen, Y.; Bouvet, M.; Sizun, T.; Gao, Y.; Plassard, C.; Lesniewska, E.; Jiang, J. Facile Approaches to Build Ordered Amphiphilic Tris (Phthalocyaninato) Europium Triple-Decker Complex Thin Films and Their Comparative Performances in Ozone Sensing. *Phys. Chem. Chem. Phys.* **2010**, *12* (39), 12851−12861.
(37) Sun, X.; Li, R.; Wang, D.; Dou, J.; Zhu, P.; Choi, C.; Cheng, D.; Ng, D.; Kobayashi, N.; Jiang, J. Synthesis and Characterization of Mixed Phthalocyaninato and meso-Tetrakis(4-chlorophenyl)-porphyrinato Triple-Decker Complexes-Revealing The Origin of Their Electronic Absorptions. *Eur. J. Inorg. Chem.* **2004**, *19*, 3806−3813.
(38) Ma, P.; Chen, Y.; Bian, Y.; Jiang, J. Morphology Controlled Surface-Assisted Self-Assembled Microtube Junctions and Dendrites of Metal Free Porphyrin-Based Semiconductor. *Langmuir* **2010**, *26* (5), 3678−3684.
(39) Chen, Y.; Chen, L.; Qi, G.; Wu, H.; Zhang, Y.; Xue, L.; Zhu, P.; Li, X. Self-Assembled Organic-Inorganic Hybrid Nanocomposite of a Perylenetetracarboxylic Diimide Derivative and CdS. *Langmuir* **2010**, *26* (15), 12473−12478.
(40) Iverson, I. K.; Casey, S. M.; Seo, W.; Tam-Chang, S.-W.; Pindzola, B. A. Controlling Molecular Orientation in Solid Films via Self-Organization in the Liquid-Crystalline Phase. *Langmuir* **2002**, *18* (9), 3510−3516.
(41) Nagata, N.; Kugimiya, S.; Kobuke, Y. Antenna Functions of 5,15-Bis (imidazol-4-yl)-10,20-bis(4-dodecyloxyphenyl)-porphyrin Supramolecular Assembly through Imidazole-Imidazole Hydrogen Bonding. *Chem. Commun.* **2000**, 1389−1390.
(42) Czikklely, V.; Forsterling, H. D.; Kuhn, H. Extended Dipole Model for Aggregates of Dye Molecules. *Chem. Phys. Lett.* **1970**, *6* (3), 207−210.
(43) Chen, Y.; Liu, H.; Zhu, P.; Zhang, Y.; Wang, X.; Li, X.; Jiang, J. Aggregation Behavior of Heteroleptic Tris(phthalocyaninato) Dysprosium Complexes with Different Alkoxy Chains in Monolayer or Multilayer Solid Films. *Langmuir* **2005**, *21* (24), 11289−11295.
(44) Liu, H.; Qian, D.; Feng, X.; Xue, Q.; Yang, K. Monolayer Studies on an Acetic Acid Substituted Porphyrin and Its Complexes with Aliphatic Amines or Quaternary Ammonium Salts at The Air-Liquid Interface. *Langmuir* **2000**, *16* (11), 5079−5085.
(45) Sui, G.; Orbulescu, J.; Mabrouki, M.; Micic, M.; Leblanc, R. M. Self-Assembly of Liquid Crystal Semiconductor Molecules at The Air/Water Interface. *J. Phys. Chem. B* **2002**, *106* (36), 9335−9340.
(46) Kasha, M.; Rawls, H. R.; EI-Bayoumi, M. A. The Exciton Model in Molecular Spectroscopy. *Pure Appl. Chem.* **1965**, *11*, 371−392.
(47) Li, G.; Ye, S.; Morita, S.; Nishida, T.; Osawa, M. Hydrogen Bonding on The Surface of Poly (2-methoxyethyl acrylate). *J. Am. Chem. Soc.* **2004**, *126* (39), 12198−12199.
(48) Génin, F.; Quilés, F.; Burneau, A. Infrared and Raman Spectroscopic Study of Carboxylic Acids in Heavy Water. *Phys. Chem. Chem. Phys.* **2001**, *3* (6), 932−942.
(49) Imahori, H.; Liu, J.-C.; Hotta, H.; Kira, A.; Umeyama, T.; Matano, Y.; Li, G.; Ye, S.; Isosomppi, M.; Tkachenko, N. V.; Lemmetyinen, H. Hydrogen Bonding Effects on The Surface Structure and Photoelectrochemical Properties of Nanostructured SnO_2 Electrodes Modified with Porphyrin and Fullerene Composites. *J. Phys. Chem. B* **2005**, *109* (39), 18465−18474.
(50) Jones, B. A.; Ahrens, M. J.; Yoon, M.-H.; Facchetti, A.; Marks, T. J.; Wasielewski, M. R. High-Mobility Air-Stable n-Type Semiconductors with Processing Versatility: Dicyanoperylene-3,4:9,10-bis(dicarboximides). *Angew. Chem.* **2004**, *116* (46), 6523−6526.
(51) Wu, W.; Liu, Y.; Wang, Y.; Xi, H.; Gao, X.; Di, C.; Yu, G.; Xu, W.; Zhu, D. High-Performance, Low-Operating-Voltage Organic Field-Effect Transistors with Low Pinch-Off Voltages. *Adv. Funct. Mater.* **2008**, *18* (15), 810−815.
(52) Kim, J. H.; Yun, S. W.; An, B.-K.; Han, Y. D.; Yoon, S.-J.; Joo, J.; Park, S. Y. Remarkable Mobility Increase and Threshold Voltage Reduction in Organic Field-Effect Transistors by Overlaying Discontinuous Nano-Patches of Charge-Transfer Doping Layer on Top of Semiconducting Film. *Adv. Mater.* **2013**, *25* (5), 719−724.
(53) Wang, Z.; Cohen, S. M. Postsynthetic Covalent Modification of a Neutral Metal-Organic Framework. *J. Am. Chem. Soc.* **2007**, *129* (41), 12368−12369.
(54) An, N.; Shi, Y.; Feng, J.; Li, D.; Gao, J.; Chen, Y.; Li, X. n-Channel Organic Thin-Film Transistors Based on a Soluble Cyclized Perylene Tetracarboxylic Diimide Dimer. *Org. Electron.* **2013**, *14* (4), 1197−1203.
(55) Oh, J. H.; Liu, S. H.; Bao, Z.; Schmidt, R.; Wurthner, F. Air-Stable n-Channel Organic Thin-Film Transistors with High Field-effect Mobility Based on N,N-bis(heptafluorobutyl)-3,4:9,10-Perylene Diimide. *Appl. Phys. Lett.* **2007**, *91* (21), 212107.

DOI: 10.1021/acsami.5b12368
ACS Appl. Mater. Interfaces 2016, 8, 6174−6182